EPSC Abstracts
Vol. 10, EPSC2015-158, 2015
European Planetary Science Congress 2015

Thermal-Gravitational Wind Equation for the Wind-Induced Gravitational Signature of Jupiter and Saturn

K. Zhang (1), D. Kong (1) and G. Schubert (2)
(1) Center for Geophysical and Astrophysical Fluid Dynamics and Department of Mathematical Sciences, University of Exeter, UK (K.Zhang@exeter.ac.uk / Fax: +44 1392 217965)
(2) Department of Earth, Planetary and Space Sciences, University of California, Los Angeles, CA 90095-1567, USA (schubert@ucla.edu)

Abstract

The thermal wind equation has been used to calculate the external gravitational signature produced by zonal winds in the interiors of Jupiter and Saturn. We show however that in this application the thermal wind equation needs to be generalized to account for an associated gravitational perturbation. We refer to the generalized equation as the thermal-gravitational wind equation. The generalized equation represents a two-dimensional kernel integral equation with the Green's function in its integrand and is hence much more difficult to solve than the standard thermal wind equation. We develop an extended spectral method for solving the thermal-gravitational wind equation in spherical geometry. We then apply the method to a generic gaseous Jupiter-like object with idealized zonal winds. We demonstrate that solutions of the thermal-gravitational wind equation are substantially different from those of the standard thermal wind equation. We conclude that the thermal-gravitational wind equation must be used to estimate the gravitational signature of deep zonal winds in giant gaseous planets.

1. Introduction

Two different approaches have been adopted to compute the wind-induced density anomaly in the deep interiors of Jupiter, Saturn and the corresponding external gravitational signatures. The computed gravitational signatures, in turn, will be used to interpret the high-precision measurements of the external gravitational fields of Jupiter and Saturn to be carried out by the Juno and Cassini spacecrafts. The first approach is based on *the thermal wind equation* (the TWE) [2, 3, 4], a diagnostic relation given by

$$\rho' = C(r) + \frac{2r\Omega}{g_{static}(r)} \int_{\pi/2}^{\theta} \Big[\cos\tilde{\theta} \frac{\partial}{\partial r} (\rho_{static} U) - \frac{\sin\tilde{\theta}}{r} \frac{\partial}{\partial \tilde{\theta}} (\rho_{static} U) \Big] \mathrm{d}\tilde{\theta}, \quad (1)$$

where $U(r,\theta)$ denotes the zonal winds, $\rho'(r,\theta)$ is the wind-induced density perturbation, $\boldsymbol{g}_{static} = \hat{\mathbf{r}} g_{static}(r)$ and $C(r)$ denotes an arbitrary function of r. The second approach makes the barotropic assumption – the density in fully compressible gaseous planets is a function only of the pressure. The barotropic model was adopted to study the effect of deep zonal winds on Jupiter's gravitational harmonics in spherical geometry [1] and in non-spherical geometry [5, 6].

We show, via both mathematical analysis and the numerical computation of simple models, that the TWE given by (1) is, in general, not valid for determining the density perturbation $\rho'(r,\theta)$ induced by deep zonal winds in giant gaseous planets such as Jupiter and Saturn. We point out that zonal flow produces not only the density perturbation ρ' but also a concomitant gravitational perturbation $\boldsymbol{g}'(r,\theta)$ to the hydrostatic gravitational force $\boldsymbol{g}_{static}$. In terms of the mathematical formulation, an extra term representing the gravitational perturbation $\boldsymbol{g}'$ produced by the interior density perturbation ρ' is of the same order of magnitude and, hence, must be retained. We then show that retaining the gravitational perturbation $\boldsymbol{g}'$ leads to *the thermal-gravitational wind equation* (TGWE), a two-dimensional kernel integral equation which, in contrast to the TWE (1), is much more difficult to solve. Through an analytical model for $\rho_{static}(r)$ in spherical geometry, the results of our calculation demonstrate that solutions of the TGWE are substantially different from those of the TWE and that the TWE, in general, cannot provide a reasonable approximation to the TGWE.

2. Derivation of the TGWE

Upon assuming that giant gaseous planets with mass M are isolated and rotating about the z-axis with angular velocity $\Omega\hat{\boldsymbol{z}}$, the governing equations in the rotating frame of reference are

$$2\Omega\hat{\boldsymbol{z}}\times\boldsymbol{u} = -\frac{1}{\rho}\boldsymbol{\nabla}p+\boldsymbol{g}+\frac{\Omega^2}{2}\boldsymbol{\nabla}\left|\hat{\boldsymbol{z}}\times\boldsymbol{r}\right|^2, \quad (2)$$

$$\boldsymbol{\nabla}\cdot(\boldsymbol{u}\rho) = 0, \quad (3)$$

where $\boldsymbol{u}(\boldsymbol{r})$ represents the velocity of the zonal winds, $\boldsymbol{r}$ denotes the position vector with the origin at the center of figure, $p(\boldsymbol{r})$ is the pressure and $\rho(\boldsymbol{r})$ is the density. Suppose that the speed of the zonal flow $\boldsymbol{u}$ is small compared to the rotation speed of the planet, equations (2)–(3) can be then solved by making use of the expansions

$$\begin{aligned} p &= p_{static}(r,\theta)+p'(r,\theta),\\ \rho &= \rho_{static}(r,\theta)+\rho'(r,\theta),\\ \boldsymbol{g} &= \boldsymbol{g}_{static}(r,\theta)+\boldsymbol{g}'(r,\theta), \end{aligned}$$

where the leading-order solution, ($p_{static}, \rho_{static}$ and $\boldsymbol{g}_{static}$), represents the hydrostatic state of the rotating gaseous planet while $(p', \rho', \boldsymbol{g}')$ denotes the perturbations arising from the effect of the zonal winds $\boldsymbol{u}$.

The second-order problem, which describes the density anomaly ρ' induced by the deep zonal flow $\boldsymbol{u}$ and the concomitant gravitational perturbation $\boldsymbol{g}'$ directly produced by ρ', is governed by the equations

$$2\rho_{static}\left(\Omega\hat{\boldsymbol{z}}\times\boldsymbol{u}\right) = -\boldsymbol{\nabla}p'+\boldsymbol{g}_{static}\rho'+\boldsymbol{g}'\rho_{static}, \quad (4)$$

$$0 = \boldsymbol{\nabla}\cdot(\boldsymbol{u}\rho_{static}). \quad (5)$$

In deriving (4) – (5), we have neglected the small high-order terms which are of $\mathrm{O}(|\boldsymbol{g}'\rho'|)$ and $\mathrm{O}(|\boldsymbol{u}\rho'\Omega|)$ and we have assumed that Ω is moderately small such that the term $(\rho'\Omega^2/2)\boldsymbol{\nabla}\left|\hat{\boldsymbol{z}}\times\boldsymbol{r}\right|^2$ can be neglected. It is critically important to notice that the terms $\boldsymbol{g}_{static}\rho'$ and $\boldsymbol{g}'\rho_{static}$ in (4) are generally of the same order of magnitude. This is because

$$\begin{aligned} |\boldsymbol{g}_{static}\rho'| &\sim \left|\rho'\boldsymbol{\nabla}\left[\int_0^{\pi}\int_0^{\widetilde{R}(\tilde{\theta})}\frac{\tilde{r}^2\sin\tilde{\theta}\rho_{static}}{|\boldsymbol{r}-\tilde{\boldsymbol{r}}|}\,\mathrm{d}\tilde{r}\,\mathrm{d}\tilde{\theta}\right]\right|\\ &= \mathrm{O}\left(\rho'\rho_{static}\right); \quad (6)\\ |\boldsymbol{g}'\rho_{static}| &\sim \left|\rho_{static}\boldsymbol{\nabla}\left[\int_0^{\pi}\int_0^{\widetilde{R}(\tilde{\theta})}\frac{\tilde{r}^2\sin\tilde{\theta}\rho'}{|\boldsymbol{r}-\tilde{\boldsymbol{r}}|}\,\mathrm{d}\tilde{r}\,\mathrm{d}\tilde{\theta}\right]\right|\\ &= \mathrm{O}\left(\rho'\rho_{static}\right). \quad (7) \end{aligned}$$

Physically, it simply means that, when the internal density anomaly ρ' is induced by the deep flow $\boldsymbol{u}$, the hydrostatic gravitational force $\boldsymbol{g}_{static}$ must be also perturbed to yield the concomitant gravitational perturbation $\boldsymbol{g}'$. Upon making a spherical approximation, we obtain

$$\begin{aligned} &2\Omega\int_{\pi/2}^{\theta}\left[\cos\tilde{\theta}\frac{\partial}{\partial r}-\frac{\sin\tilde{\theta}}{r}\frac{\partial}{\partial\tilde{\theta}}\right](\rho_{static}U)\,\mathrm{d}\tilde{\theta}\\ &= \frac{g_{static}(r)}{r}\rho'(r,\theta)-\frac{2\pi Gq(r)}{r}\\ &\times\int_0^{\pi}\int_0^{R_s}\frac{\tilde{r}^2\rho'(\tilde{r},\tilde{\theta})}{|\boldsymbol{r}-\tilde{\boldsymbol{r}}|}\sin\tilde{\theta}\,\mathrm{d}\tilde{r}\,\mathrm{d}\tilde{\theta}+C(r), \quad (8) \end{aligned}$$

where $\boldsymbol{r} = \boldsymbol{r}(r,\theta)$, $\tilde{\boldsymbol{r}} = \tilde{\boldsymbol{r}}(\tilde{r},\tilde{\theta})$ and $C(r)$ is an arbitrary function of r. Equation (8) represents a two-dimensional kernel integral equation which is referred to as *the thermal-gravitational wind equation* (TGWE). The two-dimensional kernel integral TGWE (8) that contains the Green's function $1/|\boldsymbol{r}-\tilde{\boldsymbol{r}}|$ in its integrand can be solved by an extended spectral method [7].

3. The TWE vs. the TGWE

We demonstrate that the solution of the TGWE (8) differs substantially from that of the TWE (1) for exactly the same model and parameter values and, hence, the TWE cannot generally provide a reasonable approximation to the TGWE. For this purpose, we introduce three characteristic quantities for measuring the difference between the TWE and TGWE solutions First, we introduce the norm Δ_{diff} defined as

$$\Delta_{\mathrm{diff}} = \frac{||\rho'_{\mathrm{TGWE}}(\boldsymbol{r})-\rho'_{\mathrm{TWE}}(\boldsymbol{r})||_2}{||\rho'_{\mathrm{TWE}}(\boldsymbol{r})||_2},$$

where the solution ρ' of the TWE (1) is denoted as ρ'_{TWE}, the solution ρ' of the TGWE (8) as ρ'_{TGWE} and

$$||F||_2 = \left[\int_0^{2\pi}\int_0^{\pi}\int_0^{R_s}|F(\boldsymbol{r})|^2\,r^2\sin\theta\,\mathrm{d}r\,\mathrm{d}\theta\,\mathrm{d}\phi\right]^{1/2},$$

to measure the difference between ρ'_{TGWE} and ρ'_{TWE}. The second characteristic quantity, adopted in the case of an equatorially antisymmetric wind, is the distance Δz between the center of mass and the center of figure caused by the wind-induced density anomaly. The third characteristic quantity, adopted in the case of an equatorially symmetric wind, is the lowermost coefficient $(J_2)_{\mathrm{TGWE}}$ computed from ρ'_{TGWE} and $(J_2)_{\mathrm{TWE}}$ from ρ'_{TWE}. We found, for a typical Jupiter-like model

with the deep zonal winds, that

$$\frac{||\rho'_{\rm TGWE}(\boldsymbol{r}) - \rho'_{\rm TWE}(\boldsymbol{r})||_2}{||\rho'_{\rm TWE}(\boldsymbol{r})||_2} = {\rm O}(100\%),$$

$$\frac{[(\Delta z)_{\rm TGWE} - (\Delta z)_{\rm TWE}]}{(\Delta z)_{\rm TWE}} = {\rm O}(100\%),$$

and

$$\frac{[(J_2)_{\rm TGWE} - (J_2)_{\rm TWE}]}{(J_2)_{\rm TWE}} = {\rm O}(100\%).$$

It reconfirms the result of the order-of-magnitude analysis: the gravitational perturbation term in the TGWE (8) neglected in the TWE (1) generally makes a leading-order contribution and, hence, must be retained.

4. Summary and Conclusion

The present study shows that the TWE (1) is generally incorrect for the purpose of computing the gravitational signature of a giant gaseous planet caused by the zonal winds in its deep interior. This is because an extra term representing the concomitant gravitational perturbation $\boldsymbol{g}'$ produced by the density anomaly ρ' is of the same order of magnitude and, hence, must be retained, leading to the TGWE (8).

There exist, however, two special circumstances in which the kernel integral in the TGWE (8) can be neglected and, consequently, the TWE (1) provides a good approximation to the TGWE (8). The first circumstance is when the interior fluid of a planet is weakly compressible everywhere, *i.e.*,

$$\left|\frac{1}{\rho_{static}(r)}\frac{{\rm d}\rho_{static}(r)}{{\rm d}r}\right| \ll 1 \ \text{ in } \ 0 < r < R_s.$$

However, this case does not represent the typical interior of a giant gaseous planet like Jupiter which is believed to be strongly compressible. The second circumstance is when the zonal winds U and the corresponding wind-induced density perturbation ρ' are primarily confined within a very thin outer layer defined by $(R_s - \epsilon) \leq r \leq R_s$ with $0 < (\epsilon/R_s) \ll 1$. However, this case represents an uninteresting trivial case not only because we are concerned with how a deep wind induces an externally measurable gravitational signature but also because it is obvious that $\Delta J_n^{dyn} \to 0$ when $(\epsilon/R_s) \to 0$.

References

[1] Hubbard, W. B. 1999, Icarus, 137, 357

[2] Kaspi, Y., Hubbard, W. B., Showman, A. P., & Flierl, G. R. 2010, Geophys. Res. Lett., 37, L01204

[3] Kaspi, Y., 2013, Geophys. Res. Lett., 40, 676-680

[4] Kaspi Y., Showman, A.P., Hubbard, W.B., Aharonson, O. and Helled R., 2013, Nature, 497, 344-347.

[5] Kong, D., Liao, X., Zhang, K. and Schubert, G., 2013. Icarus, 226, 1425

[6] Kong, D., Liao, X., Zhang, K. and Schubert, G., 2014. ApJ, 791, L24

[7] Zhang, K. Kong, D. and Schubert, G., ApJ (In review)

EPSC Abstracts
Vol. 10, EPSC2015-194, 2015
European Planetary Science Congress 2015

Observations of Jupiter at 5 micron from IRTF/TEXES: latitudinal variability of disequilibrium species

P. Drossart (1), T. Encrenaz (1), T.K. Greathouse (2), C. DeWitt (3), T. Fouchet (1), M. Janssen (4), S. Gulkis (4), G.S. Orton (4), L.Fletcher (5), R. Giles(5), S.K. Atreya (6), and V. Boudon (7)
(1) LESIA, Observatoire de Paris, CNRS, UPMC, Univ. Paris Diderot, Meudon, France, (2) SwRI, Div. 15, San Antonio, Texas USA, (3) Physics Department, University of California Davis, California, USA, (4) JPL, Pasadena, California, USA, (5) Clarendon Laboratory, Oxford Univ., Oxford, UK (6) Dept. of Atmospheric, Oceanic Space Sciences, University of Michigan, Ann Arbor, Michigan, USA, (7) Laboratoire Interdisciplinaire Carnot de Bourgogne, CNRS, Université Bourgogne-Franche Comté, Dijon, France (pierre.drossart@obspm.fr / Fax: +33-1-450-779-59)

Abstract

Observations of Jupiter in the 5 µm spectral window, obtained in March/April 2015 at IRTF are presented, in preparation of the arrival of the NASA/JUNO mission in 2016. Sounding of the troposphere of Jupiter below 2 bars is obtained from the observations, to search for the variability of disequilibrium species, related to deep atmospheric circulation.

1. Introduction

In preparation of the JUNO observations of Jupiter in 2016, imaging spectroscopic observations were performed between March 31 and April 4, 2015 on IRTF with TEXES (Texas Echelon Cross Echelle Spectrograph) instrument [1] in 5-12 µm range to search for composition variability over the Jovian disk. The spectral resolving power was ~13500, and radiometric calibration was done using standard procedures of the instrument.

2. Observations and modeling

This work presents the 5-micron part of the observations, and preliminary interpretation, in the following spectral ranges:

- 1931-1941 cm^{-1} (NH_3)
- 2027-2045 cm^{-1} (PH_3, CH_3D, NH_3)
- 2140-2150 cm^{-1} (PH_3, CH_4 faint lines)
- 2152-2169 cm^{-1} (PH_3, CH_3D, CO, GeH_4)

A standard radiative transfer model with simplified cloud opacities is used in this study. Thermal emission is calculated through a standard atmospheric model derived from Galileo observations [4]. A complication in atmospheric inversion comes from cloud opacities, which can affect the formation of lines. As confirmed from Galileo/NIMS interpretation at 5 micron, the simplification of a grey opacity cloud layer reproduces very well the spectral shape and can be used in a first approach [2].

3. Interpretation

Variability of tropospheric constituents are expected from different origins:

- Condensable species (NH_3, H_2O) exhibit strong variability related to local meteorological conditions, in particular in convective active regions, like the 5 µm hot spots [3].

- Disequilibrium species (PH_3, CO, GeH_4, AsH_3) could trace deeper atmospheric variability, as the transport of these species from the quenching temperature depth is dependent on the vertical mixing of the atmosphere.

4. Figures

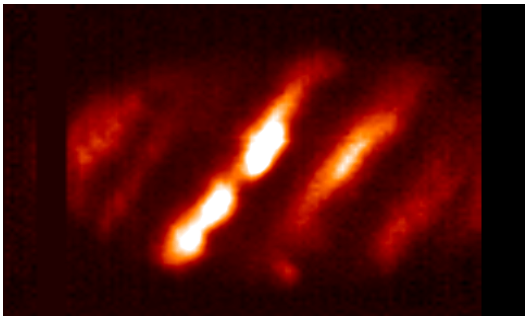

Figure 1: Image of Jupiter at 2034 cm^{-1} wavenumber (continuum) – 31/3/2015-IRTF/TEXES

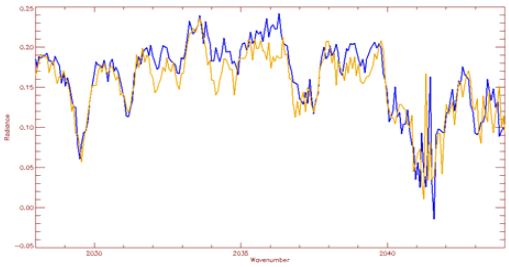

Figure 2: Two spectra selected from Jupiter at ~50N and~50S latitudes from Fig.1 spectral image. Variations in spectral absorption for a similar continuum level suggests a variation in the PH_3 abundance spatially, and hence a variation of turbulent mixing.

5. Summary and Conclusions

Preliminary models show that variability in PH_3 tropospheric abundance is present. The most plausible interpretation for such a variation would be a latitudinal variation of vertical mixing between quenching temperature levels for PH_3 stability, related to the anisotropies of convection in a rotating atmosphere.

Acknowledgements

TKG, TE and PD were visiting astronomers at the Infrared Telescope Facility, which is operated by the University of Hawaii under Cooperative Agreement no. NNX-08AE38A with the National Aeronautics and Space Administration, Science Mission Doctorate, Planetary Astronomy Program. We thank the IRTF staff for the support of TEXES observations. TKG acknowledges support of NASA grant NNX14AG34G.

References

[1] Lacy, J. H., Richter, M. J., Greathouse, T. K., Jaffe, D. T., Zhu, Q., TEXES: A Sensitive High-Resolution Grating Spectrograph for the Mid-Infrared, The Publications of the Astronomical Society of the Pacific, Vol. 114, pp. 153-168, 2002.

[2] Roos-Serote, M., Drossart, P., Encrenaz, Th., Carlson, R. W., Leader, F., Constraints on the Tropospheric Cloud Structure of Jupiter from Spectroscopy in the 5-mum Region: A Comparison between Voyager/IRIS, Galileo-NIMS, and ISO-SWS Spectra, Icarus, Vol. 137, pp. 315-340, 1999.

[3] Roos-Serote, M., Vasavada, A. R., Kamp, L., Drossart, P., Irwin, P., Nixon, C., Carlson, R. W. Proximate humid and dry regions in Jupiter's atmosphere indicate complex local meteorology, Nature, Vol. 405, pp. 158-160, 2000.

[4] Seiff, A., Kirk, D. B., Knight, T. C. D., Young, R. E., Mihalov, J. D., Young, L. A., Milos, Frank S., Schubert, G., Blanchard, R. C., Atkinson, D.: Thermal structure of Jupiter's atmosphere near the edge of a 5-µm hot spot in the north equatorial belt, Journal of Geophysical Research, Vol. 103, pp. 22857-22890, 1998.

EPSC Abstracts
Vol. 10, EPSC2015-239, 2015
European Planetary Science Congress 2015

Dynamo models for Jupiter and Saturn

C.A. Jones, W. Dietrich
Department of Applied Mathematics, University of Leeds, Leeds, UK (CAJones@maths.leeds.ac.uk)

Abstract

Jupiter's dynamo is modelled using the anelastic convection-driven dynamo equations. The reference state model is taken from French et al. 2012, which used density functional theory to compute the equation of state and the electrical conductivity in Jupiter's interior. Jupiter's magnetic field is approximately dipolar, but self-consistent dipolar dynamo models are rather rare when the large variation in density and the effective internal heating are taken into account. Jupiter-like dipolar magnetic fields were found here at small Prandtl number, $Pr = 0.1$. Strong differential rotation in the dynamo region tends to destroy a dominant dipolar component, but when the convection is sufficiently supercritical it generates a strong magnetic field, and the differential rotation in the electrically conducting region is suppressed by the Lorentz force. This allows a magnetic field to develop which is dominated by a steady dipolar component. This suggests that the strong zonal winds seen at Jupiter's surface cannot penetrate significantly into the dynamo region, which starts approximately 7000 km below the surface. Saturn's magnetic field presents more challenges, as the observed field is nearly axisymmetric and the ratio of the dipole to the octupole component suggests that in the magnetic core the field is concentrated near the polar regions. It seems likely that a stably stratified layer above the dynamo region is necessary for a successful Saturn dynamo model.

1. Introduction

Our model for Jupiter assumes a rocky inner core of radius 6700 km. For computational reasons the model is cut off 3000km below the surface, so the outermost regions, where the fluid is electrically non-conducting, are omitted. Our heating model assumes Jupiter releases uniform specific entropy as it cools through a succession of adiabats. The electrical conductivity is taken from French et al. 2012. The model assumes that Jupiter has no stably stratified layers. We integrate the anelastic equations for rotating MHD convection, using a code tested against the anelastic dynamo benchmark (Jones et al. 2011).

2. Results

We find that stable dipolar magnetic fields are much harder to find in compressible models than in Boussinesq models. However, at low Prandtl number (ratio of viscous diffusion to thermal diffusion small, as expected in Jupiter), stable dipolar fields resembling the Jovian field are found, see figure 1 (Jones, 2014).

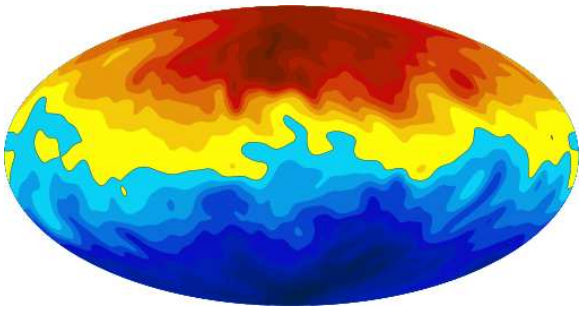

Figure 1: Simulation of the surface radial magnetic field of Jupiter.

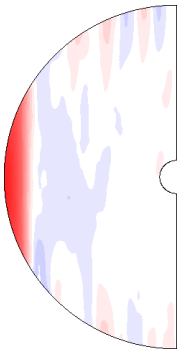

Figure 2: Meridional section of the axisymmetric component of the azimuthal flow.

To obtain a stable dipole field it is necessary that the field is strong enough to suppress the differential

rotation in the electrically conducting region. If the field is weak, strong differential rotation gives rise to dynamo waves, which preclude Jupiter-like fields. A strong zonal flow which is independent of z, the coordinate parallel to the rotation axis, is found outside the tangent cylinder surrounding the electrically conducting dynamo region, in the equatorial zone: see figure 2. This zonal flow arises from the action of Reynolds' stresses arising from the nonmagnetic rotating convection in this region.

3. Conclusions

Our estimate of the convective velocity is of order 10^{-3} m/sec, consistent with the velocity required to transport the observed heat flux. A larger value would give rise to a secular variation greater than that which occurs on Jupiter. Our models suggest that the differential rotation is not much larger than the convective velocity in the electrically conducting region, at depths below 7000 km under the surface. Outside the tangent cylinder, convection can give rise to much larger zonal flows, so within latitude $\sim \pm 26^\circ$ the zonal flow could be geostrophic and therefore deep. At higher latitudes, it is not possible for a large zonal flow to be constant on cylinders whose axis is parallel to the rotation axis, because these cylinders cut the electrically conducting region where there is only weak zonal flow. The zonal flow at high latitudes must therefore be ageostrophic, and so most likely is confined to a shallow stably stratified layer.

Reference state models for Saturn based on *ab initio* calculations are not yet available, so currently we are using models scaled from Jovian values for the electrical conductivity. Work is still in progress on Saturn's dynamo, but initial results indicate that for steady, nearly axisymmetric, anelastic dynamos, we need a convectively stable layer above the dynamo region. Provided the differential rotation in this stable layer can be maintained, the non-axisymmetric field components that must be part of the full magnetic field (Cowling's theorem) can be smoothed out, leaving only the axisymmetric part visible at the surface (Stevenson, 1982).

Acknowledgements

We acknowledge the support of the UK research Council, STFC, grant number ST/K000853/1.

References

[1] French, M., Becker, A., Lorenzen, W., Nettelmann, N., Bethkenhagen, M., Wicht, J. and Redmer, R.: Ab initio simulations for material properties along the Jupiter adiabat, Astrophys. J. Suppl., Vol. 205:5, (11pp), 2012.

[2] Jones, C.A.: A dynamo model of Jupiter's magnetic field, Icarus, Vol. 241, pp. 148-159, 2014.

[3] Jones, C.A., Boronski, P., Brun, A.S., Glatzmaier, G.A., Gastine, T., Miesch, M.S. and Wicht, J.: Anelastic convection-driven dynamo benchmarks, Icarus, Vol. 216, pp. 120-135, 2011.

[4] Stevenson, D.J. : Reducing the non-axisymmetry of a planetary dynamo and an application to Saturn, Geophys. Astrophys. Fluid Dyn., Vol. 21, pp113–127, 1982.

EPSC Abstracts
Vol. 10, EPSC2015-240, 2015
European Planetary Science Congress 2015

Solar wind-Magnetosphere-Ionosphere Coupling and Aurora at Jupiter and Saturn

E. J. Bunce and S.W.H. Cowley
University of Leicester, Department of Physics and Astronomy, Leicester, UK (ejb10@le.ac.uk)

Abstract

Solar wind-magnetosphere-ionosphere coupling is accomplished through the existence of large-scale field-aligned currents which are generated in a source region and end in a sink region, and which transfer momentum (and energy) between the regions. Therefore, to move beyond a theoretical picture of how this works at Jupiter and Saturn we require in-situ measurements of these regions primarily in the form of magnetic field measurements, but importantly combined with in-situ plasma, plasma wave data, and remote auroral observations. Since the arrival of Cassini at Saturn in 2004 we have had many opportunities to sample the high-latitude magnetosphere and aurora and have learned a great deal about how this giant magnetosphere works. We also await the "proximal" orbit phase of Cassini where we will obtain information on the high-latitude magnetosphere very close to Saturn. In the case of Jupiter, we eagerly anticipate the first high-latitude observations from the Juno mission, due to arrive in the Jupiter system in 2016. The simultaneous observations from Cassini at Saturn in the final phase of the mission until 2017, and Juno at Jupiter during 2016/17, will be a first in planetary science, and we expect to learn a great deal about both planetary magnetospheres individually and by comparison. Here then, we will give an overview of what we have learned so far from Cassini at Saturn, and how it might apply to Juno at Jupiter.

A principal "source" of the field-aligned currents is the planetary neutral atmosphere, that at Saturn imposes both sub-corotation (and is axi-symmetric to a first approximation), as well as an m=1 rotating twin-vortex perturbation of comparable magnitude. The Cassini data have revealed that there are two separate systems in the Northern and Southern hemispheres rotating with slowly-changing separate periods.

These have been systematically studied, principally in the pre-equinox (2008) Cassini data on the nightside. The sub-corotation system of field-aligned currents consists of seasonally-dependent distributed downward currents over the whole polar region extending to slightly equatorward of the polar cap/open-closed boundary with enhanced Pedersen conductivity across the boundary, followed by a narrow (auroral) layer of upward-directed field-aligned currents on the equatorward side as the conductivity decreases. The profiles are therefore similar in principle to previous theoretical predictions, but demonstrate that the conductivity profile is as important as the angular velocity in determining the field-aligned current profile.

In addition at Saturn, planetary-period oscillation (PPO) currents flow principally in the closed field region, approximately from the polar cap/open-closed boundary inwards to ~10 R_s in the equatorial plane (with smaller currents mapping inside that to at least ~6 R_S); they are associated with cross-field currents in the magnetosphere that sweep wave-like through the sub-corotating magnetosphere, causing radial displacements of the plasma (the "cam" effect). In 2008 the field-aligned currents in the South were dominated by the southern PPO phase, while those in the North were approximately equally modulated by the North and South PPO systems, showing presence of inter-hemispheric PPO current flow.

We see a strong and obvious solar-wind effect at Saturn associated with strong compressions of

magnetosphere, whose effects are interpreted as being due to the excitation of strong, tail reconnection that strongly modulates the field-aligned currents and the auroras. The system is “trickle charged” with open flux usually over intervals of days due to system size, weak interplanetary magnetic field, and Corotating Interaction Region (CIR) morphology. It therefore seems that solar wind dynamic pressure (rather than IMF direction) plays the major role in the solar wind modifying Saturn’s magnetosphere and aurora. However, there is also evidence in dayside auroras for IMF-modulated reconnection effects in post-noon sector.

Looking to Jupiter, the evidence appears strong that the main auroral oval at Jupiter is related to corotation breakdown and associated magnetosphere-ionosphere coupling currents, although the precise details of how this works will be revealed by Juno in 2016. For example, it is not obvious whether there are solar wind compression-related effects at Jupiter similar to Saturn. Following a CIR compression at Jupiter it is clear that the aurora brightens, but it is not clear which components (main auroral oval or polar aurora) are affected. A simple application of corotation breakdown models would suggest that the field-aligned currents associated with the main auroral oval should weaken under compression (i.e. dimmer aurora), and brighten under rarefaction conditions. By comparison with Saturn, we might expect that the polar aurora (possibly related to the solar wind interaction) should be brightest under compression conditions. We need to be able to measure and distinguish between field-aligned current systems associated with magnetosphere-ionosphere (corotation) and solar wind-magnetosphere coupling, and investigate how they vary over a solar rotation. This is what Juno will measure in 2016!

We will discuss the topics discussed above, with a view to taking a forward look to the exciting new data from the Cassini proximal orbits at Saturn, and the first high-latitude data from the Juno mission at Jupiter.

EPSC Abstracts
Vol. 10, EPSC2015-287, 2015
European Planetary Science Congress 2015

Juno radio science observations to constrain Jupiter's moment of inertia

S. Le Maistre (1), W. M. Folkner (1), R.A. Jacobson (1)
(1) Jet Propulsion Laboratory, California Institute of Technology, Pasadena, CA 91109, USA
(sebastien.le.maistre@jpl.nasa.gov / Tel: +1-818-354-4381)

Abstract

Through detailed and realistic numerical simulations, the present study assesses the precision with which Juno can measure the normalized polar moment of inertia (MOI) of Jupiter. Based on Ka-band Doppler and range data, this analysis shows that the determination of the precession rate of Jupiter is by far more efficient than the previously proposed Lense-Thirring effect to determine the moment of inertia and therefore to constrain the internal structure of the giant planet with Juno.

1. Context

Because of its huge gravitational attraction, Jupiter played the primary role in the formation and evolution of our Solar system. The interior structure and composition are fundamental clues to trace back the origin of the largest gaseous planet. They are therefore essential to be known to understand our Solar System.
The moment of inertia characterizes the mass concentration towards the center of the planet. It is therefore a valuable quantity to provide constraint on the interior structure and especially on the mass and size of the hypothetic core of Jupiter.

2. The Juno mission

The Juno mission en route to Jupiter aims to study the planet's composition and interior structure, gravity field, magnetic field, and polar magnetosphere in order to investigate the origin and evolution of the giant planet [1]. The mission characteristics are summarized in Table 1. Very recently, in the course of March this year, some of these characteristics have been modified; the 11-day orbital period has been increased to 14-days and the mission duration augmented from one Earth year to about 580-days.

Table 1: Juno's characteristics

Parameter	value
Orbital period	14-days
Eccentricity	e=0.95
Inclination	i=90°
Semi-major axis	a=1670000 km
Orbital plane	close to face-on
Frequency band	Ka-band (32.5GHz)
Doppler noise	10 μm/s@60s
Tracking station	DSS-25 (34-m at Goldstone)
Tracking duration	∼6h about pericenter
Jupiter orbit insertion	July 5, 2016
Nominal mission duration	580-days
Gravity science start	Nov. 11, 2016
Gravity science end	Jan. 23, 2018
Science/Gravity operations	32/26 passes

3. Pole precession rate estimate uncertainty

Using the JPL Orbit Determination Program, we carried out a variance/covariance analysis based on simulated Ka-band Doppler measurements from the Juno mission. We account here for a large number (>300) of parameters that will affect the orbital motion of Juno, including Jupiter's mass parameter (GM) and gravity field coefficients through degree 12, as well as several non-gravitational acceleration parameters (solar pressure, Jupiter infrared radiation, outgassing) and the Jupiter orientation parameters. Figure 1 shows the expected 1-σ uncertainty evolution as a function of the mission duration for 6 different operation scenarii, quantifying thereby the impact of the variation in tracking duration and repartition before (BPJ) and after (APJ) perijove.

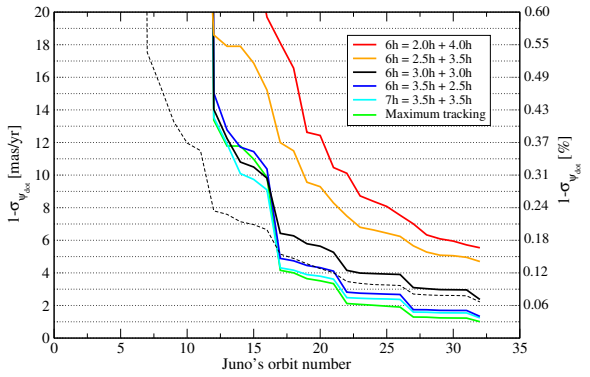

Figure 1: Time evolution of the 1-σ uncertainties in Jupiter spin axis precession rate as a function of the orbit number of Juno. The expected uncertainties obtained for each of the 6 tracking passes tested here are color-distinguished. Legends refer to tracking duration equals tracking BPJ plus tracking APJ in hours. Black thin dashed curve has been obtained with 6 hours of nominal tracking including all science pericenter passes, for comparison with the nominal black solid curve obtained with 26-gravity-dedicated passes.

4. MOI inferred uncertainty

Figure 2 shows that the normalized polar MOI will be inferred from the spin-pole precession rate of Jupiter at the same level of relative precision (i.e. $\sigma_{C/MR^2} \in [0.03\%, 0.17\%]$).

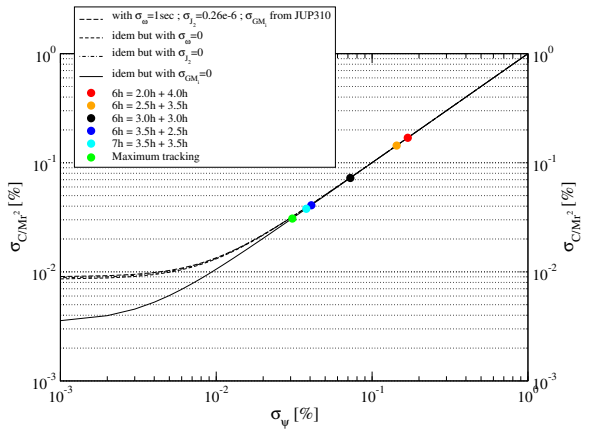

Figure 2: Jupiter's polar MOI relative precision inferred from the estimation of its pole precession rate.

5. Conclusions

We show that the determination of the pole precession rate allows for an MOI estimate about 50 times more precise than inferring it from the Lense-Thirring effect as proposed by previous studies.

In addition, we show that, given the actual tracking repartition and duration that will be performed to compute the orbit of Juno, the precision in the determination of the parameters can be increased (or decreased) by less than a factor of 3 wrt the 6h-periapsis-centered nominal tracking estimates. Such a quite small variation can however be critical in order to reach the goal of the mission and could have some consequences on the mission programmatic, depending on what will be the parameters of most interest.

We finally discuss in here the consequences of the last mission characteristic modifications (increase of the orbital period and mission duration) on the Juno's MOI estimate precision. Their implications for the detection of Jupiter's core if exists (likely) are addressed here as well as the ability to determine the core size and mass with enough precision to distinguish among competing scenarios for the planet's origin.

Acknowledgements

The research carried out at the Jet Propulsion Laboratory was supported by an appointment to the NASA Post-doctoral Program at the Jet Propulsion Laboratory, administered by Oak Ridge Associated Universities through a contract with NASA.

References

[1] S. J. Bolton. The Juno Mission. In *IAU Symposium*, volume 269 of *IAU Symposium*, pages 92–100, January 2010.

[2] R. Helled, J. D. Anderson, G. Schubert, and D. J. Stevenson. Jupiter's moment of inertia: A possible determination by Juno. *Icarus*, 216:440–448, December 2011.

EPSC Abstracts
Vol. 10, EPSC2015-292, 2015
European Planetary Science Congress 2015

Jupiter and Saturn: Two Classes of Planetary Magnetic Field

J. Bloxham (1) and S. Stanley(2)
(1) Department of Earth & Planetary Sciences, Harvard University, USA (jeremy_bloxham@harvard.edu), (2) Department of Physics, University of Toronto, Canada (stanley@utoronto.ca)

Abstract

Saturn has a nearly axisymmetric field, a morphology that is believed to be the result of a stably stratified layer surrounding the dynamo source region in which non-axisymmetric components of the field are attenuated [11]. Here we demonstrate an important theoretical consequence of such a layer, namely that the secular variation of the axisymmetric field must be extremely slow. Observational evidence suggests that this may be the case for Saturn, a finding which is supported by numerical dynamo simulations. Jupiter on the other hand has a field with significant non-axisymmetric structure and is thus not subject to constraints on its secular variation. We propose the two planets represent two different classes of planetary magnetic field: the first has nearly axisymmetric fields with very slow secular variation; the second has non-axisymmetric fields with more rapid secular variation.

1. Introduction

Saturn's magnetic field, as first revealed by Pioneer 11 [1] and the Voyager I and II spacecraft [7, 8] and more recently by the Cassini spacecraft [6], is considerably more axisymmetric than the magnetic fields of the other planets in the Solar System. For example, its dipole tilt is less than 1° [4, 5, 10] and possibly less than 0.06° [3]. In comparison, the dipole tilts of Earth and Jupiter are about 10°.

2. Secular Variation

The time-dependency of a dynamo-generated magnetic field results from one of two processes: advection of magnetic field lines by motions within the electrically conducting dynamo region and diffusion of magnetic field due to the finite electrical conductivity of the dynamo region. The effects of advection and diffusion are described by the magnetic induction equation

$$\frac{\partial \mathbf{B}}{\partial t} = \nabla \times (\mathbf{u} \times \mathbf{B}) + \eta \nabla^2 \mathbf{B} \qquad (1)$$

where $\mathbf{u}$ and $\mathbf{B}$ are the flow field and magnetic field respectively, and η is the magnetic diffusivity.

In general, for dynamo action to occur, the ratio of these two effects (the magnetic Reynolds number) must be large; however, geometrical effects may result in the effects of advection on the time-dependency of the externally observed field being small, even though the magnetic Reynolds number in the interior is large. The fact that Saturn's magnetic field is nearly axisymmetric demands that the fluid flow near the top of the dynamo region must preserve the nearly axisymmetric nature of the field. Bullard and Gellman [2] in a pioneering study of the generation of magnetic fields by dynamo action, developed a formalism for understanding this interaction of fluid flow and the magnetic field.

If we assume that the fluid flow at the top of the dynamo is purely toroidal, as required by the presence of a stably stratified layer, then using the Bullard-Gellman formalism we can show that the flows that preserve the axisymmetric nature of the field do not change the axisymmetric part of the field. In other words, the flows that preserve axisymmetry do not create secular variation. Secular variation can then only result from either much slower diffusive processes or from the advection of very weak nonaxisymmetric field components. In either case, the secular variation will be weak. We note, however, that if some secular variation of a axisymmetric field were to be observed on a timescale shorter than the diffusive timescale then an estimate could be made of the nonaxisymmetric field.

3 Remarks

Based on this analysis we propose that there are two classes of planetary magnetic fields, axisymmetric

fields with weak secular variation and nonaxisymmetric fields with strong secular variation. Saturn belongs to the first class (possibly alongside Mercury [9]) while Jupiter and Earth belong to the second class.

The Juno observations of Jupiter and the proximal Cassini observations of Saturn will provide an opportunity to test this theory.

References

[1] Acura, M. and Ness, N.:Magnetic-field of Saturn—Pioneer-11 observations, Science, Vol. 207, pp. 444-446, 1980.

[2] Bullard, E. and German, H.: Homogeneous dynamos and terrestrial magnetism, Philosophical Transactions of the Royal Society of London A, Vol. 247, pp. 213-278, 1954.

[3] Cao, H., Russell, C., Christensen, U., Dougherty, M. and Burton, M.: Saturn's very axisymmetric field: no detectable secular variation or tilt, Earth and Planetary Science Letters, Vol. 304, pp. 22-28, 2011.

[4] Connerney, J., Ness, N. and Acuna, M.: Zonal harmonic model of Saturn's magnetic field from Voyager 1 and Voyager 2 observations, Nature, Vol. 298, pp. 44-46, 1982.

[5] Connerney, J., Acuna, M. and Ness, N.: The Z3 model of Saturn's magnetic field and the Pioneer 11 vector helium magnetometer observations, Journal of Geophysical Research, Vol. 89, pp. 7541-7544, 1984.

[6] Giampieri, G. and Dougherty, M.: Rotation rate of Saturn's interior from magnetic field observations, Geophysical Research Letters, 10.1029/2004GL020194.

[7] Ness, N., Acuna, M., Connerney, J., Lepping, R., Burlaga , L. and Neubauer, F.: Magnetic-field studies by Voyager 1—Preliminary results at Saturn, Science, Vol. 212, pp. 211-217, 1981.

[8] Ness, N., Acuna, M., Behannon, K., Burlaga, L., Connerney, J., Lepping, L. and Neubauer, F.: Magnetic-field studies by Voyager 2—Preliminary results at Saturn, Science, Vol. 215, pp. 558-563, 1982.

[9] Philpott, L. and Johnson, C.: Constraints on the secular variation of Mercury's magnetic field from the combined analysis of MESSENGER and Mariner 10 data, Geophysical Research Letters, Vol. 41, pp. 6627-6634, 2014.

[10] Smith, E., Davis, L., Jones, D., Coleman, P., Colburn, D., Dyal, P. and Sonett, C.: Saturn's magnetic-field and magnetosphere, Science, Vol. 207, pp. 407-410, 1980.

[11] Stevenson, D.: Reducing the non-axisymmetry of a planetary dynamo and and application to Saturn, Geophysical and Astrophysical Fluid Dynamics, Vol. 21, pp. 113-127, 1982.

EPSC Abstracts
Vol. 10, EPSC2015-294, 2015
European Planetary Science Congress 2015

Variability in Saturn's upper atmosphere from Cassini/UVIS occultations

T. T. Koskinen (1,2), D. F. Strobel (3), R. A. West (4), B. R. Sandel (1) and R. V. Yelle (1)
(1) Lunar and Planetary Laboratory, University of Arizona, Tucson, AZ, USA, (2) Cassini participating scientist, (3) Johns Hopkins University, Baltimore, MD, USA, (4) Jet Propulsion Laboratory, California Institute of Technology, La Canada Flintridge, CA, USA (tommi@lpl.arizona.edu)

Abstract

We present new density and temperature profiles based on more than 20 stellar occultations by Saturn's upper atmosphere observed simultaneously by the EUV and FUV channels of the Cassini/UVIS instrument. With these results, more than 40 stellar and solar occultations from Cassini/UVIS [1, 2, 3] and 6 occultations from Voyager/UVS [4] have now been analyzed. The results provide valuable constraints on models of chemistry, dynamics and thermal structure in the upper atmosphere. They are also required to plan for the end of the Cassini mission.

1. Introduction

The occultations and airglow measurements of Saturn by the Voyager/UVS and Cassini/UVIS instruments constitute the most extensive dataset available on the upper atmosphere of any giant planet. For the first time, these observations can be used to probe spatial and temporal trends in the density and temperature structure of the upper atmosphere that are driven by changes in energy deposition, chemistry and dynamics. They are also required to plan the Grand Finale tour of the Cassini mission that includes several close orbits with the spacecraft passing through Saturn's thermosphere, followed by its final descent into the lower atmosphere.

Here we concentrate on the stellar occultations from the Cassini/UVIS instrument [5]. The EUV occultations are used to retrieve the H_2 density and temperature profiles in the thermosphere. The temperature in the thermosphere is generally much higher than expected from solar heating, and these observations constrain the heating mechanism. The FUV occultations, on the other hand, are used to retrieve the density profiles of minor hydrocarbons such as CH_4, C_2H_2, C_2H_4 and C_2H_6 in the upper stratosphere/mesosphere. These results provide constraints on models of photochemistry, thermal structure and dynamics [6, 7]. In fact, spatial trends in temperature and the mixing ratios of the minor species are one of the only available sources of information on circulation above the cloud tops [8].

2. Results

We present new results based on more than 20 stellar occcultations probing the atmosphere at different locations between 2004 and 2015. For each location, we construct a reference atmosphere model relying on the occultation data and observations of the stratosphere by the Cassini/CIRS instrument [9, 10]. These models allow us to convert density profiles into mixing ratios, estimate the pressure-temperature structure in Saturn's highly oblate atmosphere, and to derive values for the eddy mixing rate that depends on dynamics. Figure 1 shows an example of such a model for one of the occultations.

The EUV stellar occultations show that the exospheric temperature on Saturn ranges from about 350 K to 600 K [3], in agreement with the solar occultations [2] and the latest re-analysis of the Voyager/UVS occultations [4]. The temperature increases with latitude from the equator towards the poles, supporting the idea that high latitude (auroral) heating and the associated electrodynamics can explain the temperatures in the thermosphere. Under the assumption of gradient wind balance, which is a reasonable order of magnitude estimate in the non-auroral thermosphere, the data imply that easterly zonal jets with mid-latitude wind speeds of about 600 m s^{-1} exist in both hemispheres, consistent with high latitude heating [3].

The occultations also reveal that Saturn's equatorial thermosphere expanded by about 500 km between 2005 and 2010, followed by contraction after 2010 that may still be ongoing. These trends, that anticorrelate with solar activity, may be seasonal in nature. Since the thermosphere is not expected to re-

act directly to changes in solar insolation, the changes could be indirectly linked to changes in dynamics of the upper stratosphere/mesosphere. The hydrocarbon profiles retrieved from the FUV channel provide further constraints on chemistry and dynamics below the thermosphere.

3. Figures

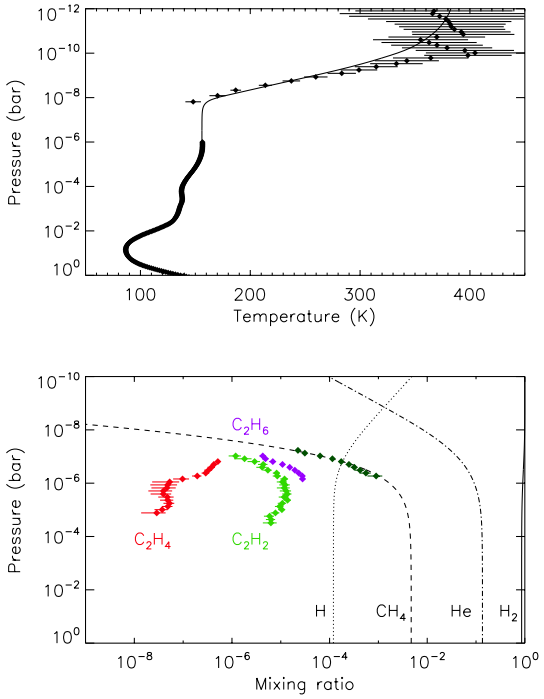

Figure 1: **Upper panel**: The solid line shows the model temperature profile based on the closest available coincidence of UVIS ($p < 10^{-8}$ bar) and CIRS ($p > 10^{-6}$ bar) data points (diamonds) from the spring of 2006 [9, 3]. The model T-P profile in the thermosphere is the best fit forward model profile fitted to the UVIS data while the data points result from direct inversion. **Lower panel**: Mixing ratios for some of the minor species. Lines show the mixing ratios in the atmosphere model that determine mean molecular weight while the data points show the retrieved number densities divided by the total density of the model atmosphere. The mixing ratio of H is limited by the solar occultations and the mixing ratio of He is uncertain (we assumed 13.55 % in the lower atmosphere).

References

[1] Shemansky, D. E., Liu, X.: Saturn upper atmospheric structure from Cassini EUV and FUV occultations, Can. J. Phys., Vol. 90, pp. 817-831, 2012.

[2] Koskinen, T. T., et al.: The density and temperature structure near the exobase of Saturn from Cassini/UVIS solar occultations, Icarus, Vol. 226, pp. 1318–1330, 2013.

[3] Koskinen, T. T., et al.: Saturn's variable thermosphere from Cassini/UVIS occultations, under review at Icarus, 2015.

[4] Vervack, R. J. Jr., Moses, J. I.: Saturn's upper atmosphere during the Voyager era: Reanalysis and modeling of the UVS occultations, arXiv:1408.1746v1, 2014.

[5] Esposito, L. W., et al.: The Cassini ultraviolet imaging spectrograph investigation, Space Sci. Rev., Vol. 115, pp. 299–361, 2004.

[6] Yelle, R. V., Griffith, C. A., Young, L. A.: Structure of the Jovian stratosphere at the Galileo probe entry site, Icarus, Vol. 152, pp. 331–346, 2001.

[7] Moses, J. I., et al.: Photochemistry and diffusion in Jupiter's stratosphere: Constraints from ISO observations and comparisons with other giant planets, J. Geophys. Res., Vol. 110, pp. E08001, 2005.

[8] Friedson, A. J., Moses, J. I.: General circulation and transport in Saturn's upper troposphere and stratosphere, Icarus, Vol. 218, 861–875, 2012.

[9] Guerlet, S., Fouchet, T., Bézard, B., Simon-Miller, A. A., Flasar, F. M.: Vertical and meridional distribution of ethane, acetylene, and propane in Saturn's stratosphere from Cassini/CIRS limb observations, Icarus, Vol. 203, pp. 214–232, 2009.

[10] Guerlet, S., Fouchet, T., Bézard, B., Flasar, F. M., Simon-Miller, A. A.: Evolution of the equatorial oscillation in Saturn's stratosphere between 2005 and 2010 from Cassini/CIRS limb data analysis, Geophys. Res. Lett., Vol. 38, pp. L09201, 2011.

EPSC Abstracts
Vol. 10, EPSC2015-350, 2015
European Planetary Science Congress 2015

Ionosphere-magnetosphere coupling studies with Juno and Cassini proximal orbits

M. Blanc (1), S. Bolton (2), F. Bagenal (3), W. S. Kurth (4), N. André, P.-L. Blelly, V. Génot, P. Louarn, A. Marchaudon, C. Peymirat, C. Tao (1)
(1) IRAP, Toulouse, France (2) SwRI, San Antonio, USA (3) LASP, Univ. Colorado, Boulder, USA (4) University of Iowa, Iowa City, USA (michel.blanc@irap.omp.eu; fax +33 5 61 55 86 92)

Abstract

The magnetodisk of Jupiter is dragged into partial cororation with the planet by a current loop that connects the disk to the jovian upper atmosphere via intense field-aligned currents driving the main auroral emissions. Thanks to its unique orbital geometry, Juno will allow for the first time a quantitative study of the characteristics of the three key segments of this circuit. To a large extent, the Cassini proximal orbits will provide a similar opportunity at Saturn. We will describe our plans for a physical study of these three segments and their interconnections, and of the key processes that are at work in the enforcement of magnetospheric corotation and sub-corotation at Jupiter and Saturn.

1. Introduction

Juno offers a unique opportunity to understand how the largest magnetosphere in the solar system works [2]. Here is only one example of the many Juno scientific opportunities.

Figure 1 illustrates the three segments composing the current loop that transfers angular momentum between thermosphere-ionosphere and magnetodisk: Segment A – the plasmasheet/magnetodisk; segment B – the high-altitude auroral field lines: segment C – the auroral thermosphere-ionosphere.

The orbits of Juno will scan through segment A over the duration of the mission. Juno will directly fly through segment B at a variety of altitudes. Finally Juno will fly over the polar and auroral thermosphere-ionosphere and will monitor the auroral emissions. The geometry of Cassini proximal orbits will allow similar encounters with our three key segments. Through the synergistic use of data and models, it will be possible to untangle the key processes in the exchange of momentum between the two ends of our circuit.

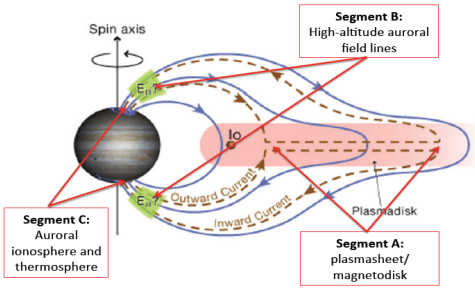

Figure 1: Geometry of the field lines and current loops that connect the magnetodisk to the ionosphere, with the three "key segments" shown.

2. Analysis of the circuit

2.1 The plasmasheet/magnetodisk

While the main "ring" current maintaining the plasmasheet magnetic field in its elongated configuration is azimuthal and produced by the pressure gradient and centrifugal forces, the current that closes the corotation-enforcing current loop is radial (e.g., figure 1). This current, related to the Coriolis force, is directly driven by the net outward radial transport of mass in the disk.

Therefore, to quantitatively evaluate this radial current, one must know first the equilibrium configuration of the plasmasheet, and then observe the different modes of radial transport developing in the disk **[1] [5]**. From a comprehensive analysis of these modes it will be possible to evaluate the net radial mass transport. By doing so, we will be able to determine the radial current in the disk (segment A).

2.2 The high-altitude auroral field lines

The closure of magnetospheric currents through the ionosphere involves intense current sheets flowing along field lines. At high altitudes, the Earth example shows that the upward currents are associated with a variety of phenomena organized at different scales: field-aligned precipitating electron beams, transversely accelerated upward-flowing ions, strong field-aligned electric potential drops, density cavities, and radio emissions that seem to develop inside these cavities before propagating in free space. At the largest latitudinal scales these phenomena seem to be controlled by the physics of closure of large-scale currents along field lines, involving a characteristic current-voltage relationship; at the smaller scales, Alfven waves interacting with the density structures would play the dominant role **[4]**.

Data from Juno and Cassini will make it possible to diagnose this host of phenomena for the first time on jovian and kronian auroral field lines, and to establish the integrated current-voltage relationship resulting from the interplay of the different scales.

2.3 The auroral ionosphere and thermosphere

Currents flowing along auroral field lines finally close in the ionosphere. Juno and Cassini will monitor the inputs to this ionosphere/thermosphere system: particle precipitation fluxes, field-aligned currents, and to some extent the intensity and geometry of auroral emissions, which will provide constraints on where and how deep the auroral energy is deposited.

With the help of thermosphere/ionosphere electrodynamic coupling models **[6] [3]**, it will then be possible to use these inputs to calculate the horizontal closure of magnetospheric currents, and the dynamic and thermodynamic response of the thermosphere to auroral forcing. This thermospheric response itself produces a feed back on magnetospheric motions, which will be evaluated **[7]**.

3. Conclusions

The regular Juno orbits, as well as the Cassini proximal orbits, provide a unique opportunity for a comprehensive study of the electrodynamic current loop that connects the plasmasheet/magnetodisk of gas giants to their auroral ionosphere and thermosphere. The three key segments of this current loop will be studied along the orbits, and analysed at a variety of scales to determine the resulting current characteristics. Closure through the ionosphere/thermosphere will be calculated with the support of specifically adapted electrodynamic models, and from that point the whole current circuit will be determined, thus resulting in a proper evaluation of the net transfers of angular momentum and energy between the magnetodisks and the upper atmospheres.

References

[1] André, N. et al., Magnetic signatures of plasma-depleted flux tubes in the Saturnian inner magnetosphere, Geophys. Res. Let.,34, 14, L14108, 2007.

[2] Bagenal, F. et al., Magnetospheric science objectives of the Juno mission, Space Sci Rev DOI 10.1007/s11214-014-0036-8, 2014.

[3] Blelly, P.-L. et al., An extended TRANSCAR model including ionospheric convection: simulation of EISCAT observations using inputs from AMIE, Ann. Geophysicae, 23, 419-431, 2005.

[4] Chaston, C. C., V. Génot, J. W. Bonnell, C. W. Carlson, J. P. McFadden, R.E. Ergun, R. J. Strangeway, E. J. Lund and K. J. Hwang, Ionospheric erosion by Alfven waves, J. Geophys. Res. March 2006, DOI: 10.1029/2005JA011367

[5] Louarn, P, C. Paranicas, P. Christopher, and W. S. Kurth, Global magnetodisk disturbances and energetic particle injections at Jupiter, J. Geophys. Res., 119, 6, 4495-4511, 2014

[6] Peymirat, C., B. Emery, A. D. Richmond, and R. G. Roble, A magnetosphere-thermosphere-ionosphere electrodynamics general circulation model, J. Geophys. Res., 103, 17467, 1998.

[7] Tao, C., H. Fujiwara, and Y. Kasaba, neutral wind control of the Jovian magnetosphere-ionosphere current system, J. Geophys. Res., 114, A08307, 2009.

EPSC Abstracts
Vol. 10, EPSC2015-363, 2015
European Planetary Science Congress 2015

Cassini at Saturn: The Final Two Years

L.J. Spilker (1), S.G. Edgington (1), and N. Altobelli (2)
(1) Jet Propulsion Laboratory/California Institute of Technology, USA (linda.j.spilker@jpl.nasa.gov), (2) ESA/ESAC, Villafranca del Castillo, Madrid, Spain

Abstract

After 11 years in orbit, the Cassini-Huygens Mission to Saturn, a collaboration of NASA, ESA, and ASI, continues to wow the imagination and reveal unprecedented findings. Every year Cassini produces answers to questions raised by the Voyager flybys, while at the same time posing new questions that can *only* be answered with a long duration mission using a flagship-class spacecraft. Here we sample a few of Cassini's discoveries from the past year and give an overview of Cassini's final two years.

1. Exploring the Saturn System

Cassini's exploration of the Saturn System is composed of five broad, overlapping scientific disciplines: Titan, the atmosphere of Saturn, rings, magnetosphere, and icy satellites (Figure 1).

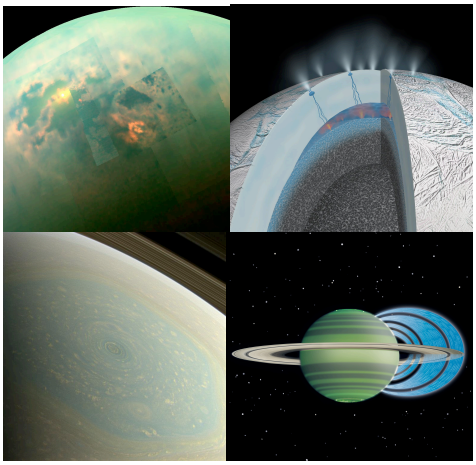

Figure 1: The five major science disciplines of the Cassini-Huygens Mission include (clockwise from upper left hand) Titan, icy satellites, magnetosphere and rings, and Saturn.

In each area, Cassini made major discoveries, provided answers to old questions, and posed new questions that may be answered in the mission's final two years. Among many firsts, Cassini: discovered icy jets of material streaming from tiny Enceladus' south pole proving that it is the source of the E Ring and that its water dominates the magnetosphere; found hydrocarbon lakes and seas on Titan; detected sub-surface oceans in Enceladus and Titan; provided multi-wavelength coverage of a great northern storm, the first of its kind on Saturn since 1990; demonstrated that the Saturn Kilometric Radiation period does not reflect the planet's internal rotation; revealed curtain-like aurorae and their true color flickering over Saturn's poles;; and constrained and complicated our understanding of the 3D structure and dynamics of multi-particle ring systems. In addition, the Huygens probe sent back amazing images of Titan's surface and made detailed measurements of atmospheric composition, structure and winds.

In just the last three years, Cassini discovered that: the majority of Titan's lakes and seas are located near the north pole; Enceladus harbors a subsurface ocean with possible hydrothermal activity where the ocean and rocky core meet; a huge hurricane rages at Saturn's north pole; tidal stresses control Enceladus' particulate jets with plume activity greatest near apoapse; the depth of Titan's Ligeia Mare is 150-200 meters; meteorite impacts, embedded propellers migrating inwards and outwards, and the effects of Saturn internal oscillations can be witnessed in the rings; Titan has a subsurface water ocean; interactions between a strong solar wind and Saturn's magnetosphere can help us understand supernovae shockwaves; Titan's south polar haze is a seasonal phenomenon; ephemeral "islands" exist in Titan's lakes; and methane ice clouds can be present in Titan's stratosphere..

Cassini continues to inform the planning of future missions. Over the next two years, Northern Summer Mission (NSM) will complete Cassini's investigation of the Saturn system throughout half the

planet's year. We will monitor seasonal changes on Saturn and Titan in a previously unobserved seasonal phase. As northern summer approaches, long-dark regions throughout the system have become sunlit with the reverse occurring in the south, allowing Cassini's science instruments to probe as-yet unsolved mysteries, observe seasonal and temporal changes, and address new questions that have arisen during the mission thus far.

2. F Ring and Proximal Orbits

The final phase of Cassini's Northern Solstice Mission covers a period of roughly ten months and will end the mission by exploring for the first time the region between the rings and planet, a rich source for discovery. It will begin with 20 orbits with periapse just outside the F Ring (Figure 2) before transitioning to 22 Proximal Orbits, with periapse between the rings and planet. The last orbit will take the spacecraft into Saturn on September 15, 2017, where it will be vaporized by the planet's atmosphere.

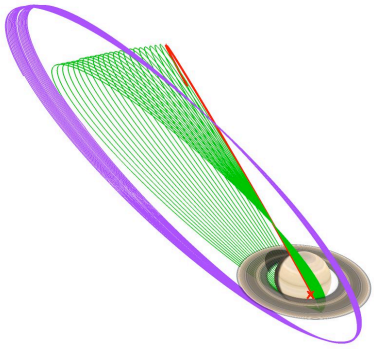

Figure 2: F Ring and Proximal Orbit phase: 20 F Ring (purple) orbits and 22 Proximal Orbits (green). The last orbit (red) will take Cassini into Saturn (red x) for vaporization by Saturn's atmosphere.

During this phase, Cassini will attempt to answer fundamental questions related to Saturn's interior structure and rotation rate, the internal magnetic field and dynamo, the total mass of the main rings, and the dust, gas, and plasma composition between the rings and planet, in addition to acquiring the mission's closest views of the rings, ring moons, aurora, and planet, revealing their detailed structure (Figure 3).

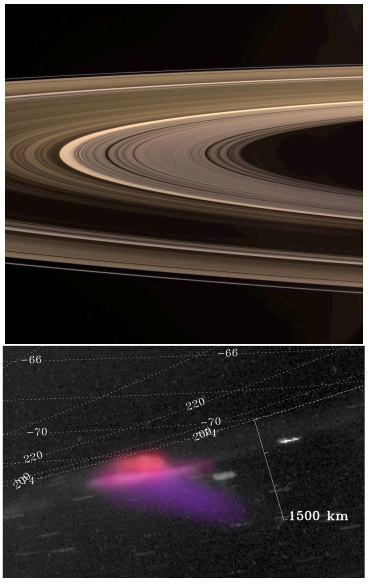

Figure 3: Image of the unlit side of the rings with the innermost, much fainter D ring (above). Saturn's aurora in true-color (below).

3. Summary and Conclusions

Cassini-Huygens exploration of Saturn has yielded 11 years of unprecedented discoveries, and answers to many scientific mysteries. The healthy spacecraft is poised to embark on the final two years with an exciting end of mission that will answer fundamental questions about Saturn, the rings and magnetosphere.

The year 2017 will be an exciting time for giant planet research, as Cassini and Juno simultaneously probe the interiors of Saturn and Jupiter. The new data will attract an array of experts in giant planet research, and the outcome will be a huge leap in understanding our two gas giants.

Acknowledgements

The research described in this paper was carried out in part at the Jet Propulsion Laboratory, California Institute of Technology, under a contract with the National Aeronautics and Space Administration. Government sponsorship is acknowledged.

EPSC Abstracts
Vol. 10, EPSC2015-476, 2015
European Planetary Science Congress 2015

The detection of Jupiter normal modes with gravity measurements of the mission Juno

D. Durante, and L. Iess

Sapienza University of Rome, Rome, Italy (daniele.durante@uniroma1.it)

Abstract

Arriving at Jupiter on July 4, 2016, NASA's Juno mission will complete 37 orbits (14-days period) around the planet, revealing details of the interior structure and composition, a crucial aspect to understand the origin and evolution of Jupiter. A radio science experiment will help to select and validate the existing models of Jupiter internal composition, in particular the mass of the silicate core.

The Juno radio science experiment exploits microwave radio link between ground stations and Juno to collect two-way range-rate measurements from the Doppler shift of a coherent Ka-band (32-34 GHz), two-way radio link. These data are processed through orbit determination codes to estimate both the position and velocity of the spacecraft at a given epoch, and additional parameters of scientific interest, such as the spherical harmonics coefficients of the gravity field. In addition, the experiment will provide an estimate of the angular momentum of Jupiter from the relativistic Lense-Thirring.

Recently it has been proposed to exploit the Doppler data for the determination of Jupiter's acoustic normal modes. Jupiter is a gaseous giant and its masses are subject to oscillations (normal modes) due to internal pressure waves, which cause potentially detectable disturbances in the gravity field. By displacing large masses, Jupiter's normal modes can therefore perturb the spacecraft motion to levels that can be measured by Juno's extremely accurate Doppler system. Theoretical models that explain these phenomena have been proposed in the past and experimental works looking for these oscillations have been carried out recently with ground-based optical telescopes. But the frequencies and the amplitudes of normal modes can in principle be modeled and estimated by means of orbit determination codes. This requires the modification of the mathematical model of the system's dynamics and the upgrade of the estimation filters.

The purpose of this study is to characterize the mathematical model that governs the normal modes of Jupiter and predict the associated power to each mode, based on published results. These works report the observation of a maximum radial velocity of the upper atmosphere of Jupiter of the order of 50cm/s at a peak frequency of 1200μHz. In this condition, the oscillation amplitude of Jupiter can potentially be so large to be observable by Juno.

In addition, the study focus on the observability conditions of the normal modes, also in relation to the spacecraft orbit geometry, and their discrimination from the static gravity field. Juno sensitivity to different dynamic gravity field coefficients at different frequencies is also being investigated. These goals are achieved by means of numerical simulations, providing in particular the estimation error, to be compared with the formal uncertainties of dynamic coefficients.

EPSC Abstracts
Vol. 10, EPSC2015-509, 2015
European Planetary Science Congress 2015

The Juno and Cassini gravity measurements: probing the interior dynamics of Jupiter and Saturn

Y. Kaspi (1), E. Galanti (1), W. B. Hubbard (2) and J. E. Davighi (1,3)
(1) Department of Earth and Planetary Sciences, Weizmann Institute of Science, Israel (yohai.kaspi@weizmann.ac.il)
(2) Lunar and Planetary Laboratory, University of Arizona, USA (3) Department of Physics, University of Cambridge, UK

Abstract

During 2016-2017 both the Juno and Cassini spacecraft will enter into close-by polar orbits of Jupiter and Saturn, respectively. Using Doppler tracking from Earth these flybys will allow high precision gravity measurements of these planets [1]. These will include high order gravity harmonics (at least up to J_{10}), and the yet to be measured odd gravity spectrum. As the dynamics of deep flows relate to perturbations in the density of the planets, this data can be used to probe for the first time the atmospheric and interior flows on these planets [4, 5, 8]. Particularly, this may allow addressing one of the longest-standing questions in planetary atmospheric dynamics regarding the depth of the observed strong east-west jets-streams on Jupiter and Saturn. In this talk we review different approaches to analyze the gravity measurements, discuss the proposed models relating the gravity fields to the dynamics, and the implications of the results for understanding the mechanisms governing the interiors and atmospheres of Jupiter and Saturn.

1. Gravity field analysis

The measured gravity field can be decomposed to a contribution from the static planet, and a contribution due to dynamics. Several approaches can be taken for inferring the dynamics from the gravity data:

1. The high-order zonal gravity harmonics are dominated by the dynamics [5]. We find that if the flow is deep enough, $O(1000$ km$)$ beneath the cloud level, then the signal of deep dynamics is measurable by the high order gravity spectra [8].

2. The odd gravity harmonics have no contribution from the static planet, and therefore any measurement of odd harmonics (J_3, J_5, J_7, etc.) will likely be a pure signature of deep dynamics (Fig. 1). We find that even flows $O(100$ km$)$ below the cloud level should produce a measurable ($O(10^{-9})$, [2]) gravity signal [7, 11].

3. Upper limits on the depth of the dynamics can be obtained by comparing low order even harmonics from dynamical models to the difference between the measured low order even harmonics and the largest possible values of a static planet. Such analysis has proved to be useful for the cases of Uranus and Neptune [9], and with sufficient accuracy by Juno and Cassini of the low order even harmonics (J_2, J_4, J_6), may be applicable to Jupiter and Saturn as well.

4. Spatially varying measurements of the gravity field enable direct probing of spatially varying dynamical features such as the equatorial jets or the Great Red Spot [13]. We show under which conditions such gravity measurements give a detectable signal.

2. Models

To date, three different types of models have been suggested to relate the measurable gravity field and the dynamical induced density perturbations: potential theory models, thermal-wind models and general circulation models. We discuss the pros and cons of each, and show how they can be compared and checked against one another. The potential theory method allows accurate solutions of the gravity field, taking into account the planetary oblateness that dominates the low-order harmonics, but is limited to only purely barotropic flows (full differential rotation) [5, 6, 10]. On the other hand, the thermal wind model allows for any type of wind field but is limited to spherical symmetry, thus allowing us to calculate only the dynamically induced components of the spectrum and neglecting non-spherical effects [8, 7, 12]. Nonetheless, we show that approximate solutions using the thermal wind method can be obtained by incorporating the

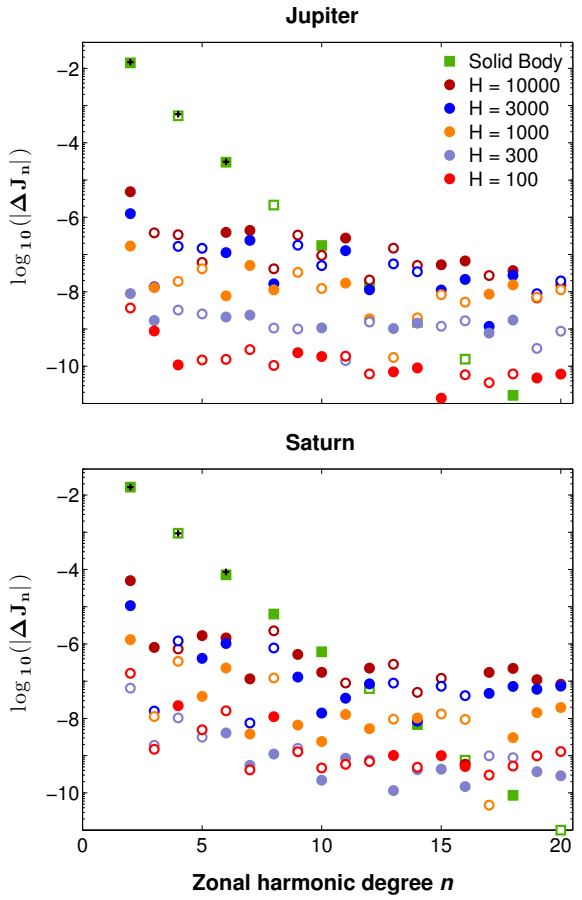

Figure 1: The static (squares) and dynamical (circles) gravity spectrum for Jupiter (top) and Saturn (bottom). The dynamical gravity harmonics are shown for five different decay depth values (H, in km) using the thermal wind model [8, 7]. Plus signs show the currently observed values of J_n. Taken from [7].

oblateness effects, and in the appropriate limits the two methods give nearly identical solutions. General circulation models contain more complete physics, but are limited to specific parameterizations and governing equations, and thus to specific types of flows that might not be representing well the exterior dynamics [8]. As eventually we would like to translate the measured gravity field into wind fields, we present also an adjoint based inversion technique to do so [3]. We show examples of how this adjoint model coupled with the thermal wind model can produce realizations of the interior flow given a measured gravity field. Finally, we discuss the implications of these measurements to understanding the mechanisms driving the dynamics on these planets.

3. Summary

The Juno and Cassini gravity measurements will provide an exciting opportunity to probe the dynamics of the atmospheres and interiors of Jupiter and Saturn. A combination of different models and methods is necessary for the data analysis. The results presented here show that it is likely that this upcoming data will provide new insights about the extent of the dynamics, and the mechanisms controlling the observed flows.

References

[1] S. J. Bolton. Juno final concept study report. Technical Report AO-03-OSS-03, New Frontiers, NASA, 2005.

[2] S. Finocchiaro and L. Iess. Numerical simulations of the gravity science experiment of the Juno mission to Jupiter. In *Spaceflight mechanics*, volume 136, pages 1417–1426. Amer. Astro. Soc., 2010.

[3] E. Galanti and Y. Kaspi. An adjoint based method for the inversion of the Juno and Cassini gravity measurements into wind fields. *Icarus*, 2015. submitted.

[4] W. B. Hubbard. Effects of differential rotation on the gravitational figures of Jupiter and Saturn. *Icarus*, 52:509–515, 1982.

[5] W. B. Hubbard. Note: Gravitational signature of Jupiter's deep zonal flows. *Icarus*, 137:357–359, 1999.

[6] W. B. Hubbard. High-precision Maclaurin-based models of rotating liquid planets. *Astrophys. J. Let.*, 756:L15, 2012.

[7] Y. Kaspi. Inferring the depth of the zonal jets on Jupiter and Saturn from odd gravity harmonics. *Geophys. Res. Lett.*, 40:676–680, 2013.

[8] Y. Kaspi, W. B. Hubbard, A. P. Showman, and G. R. Flierl. Gravitational signature of Jupiter's internal dynamics. *Geophys. Res. Lett.*, 37:L01204, 2010.

[9] Y. Kaspi, A. P. Showman, W. B. Hubbard, O. Aharonson, and R. Helled. Atmospheric confinement of jet-streams on Uranus and Neptune. *Nature*, 497:344–347, 2013.

[10] D. Kong, K. Zhang, and G. Schubert. On the variation of zonal gravity coefficients of a giant planet caused by its deep zonal flows. *Astrophys. J.*, 748, 2012.

[11] D. Kong, K. Zhang, and G. Schubert. Wind-induced odd gravitational harmonics of Jupiter. *Mon. Not. Roy. Astro. Soc.*, 450:L11–L15, 2015.

[12] J. Liu, T. Schneider, and Y. Kaspi. Predictions of thermal and gravitational signals of Jupiter's deep zonal winds. *Icarus*, 224:114–125, 2013.

[13] M. Parisi, E. Galanti, and Y Kaspi. Inferring the depth of Jupiter's Great Red Spot with the Juno gravity experiment. *Icarus*, 2015. in prep.

EPSC Abstracts
Vol. 10, EPSC2015-770, 2015
European Planetary Science Congress 2015

Science highlights from the Cassini magnetometer and focus for the end of mission orbits

Michele K. Dougherty (1) and the Cassini Magnetometer Team
(1) The Blackett Laboratory, Imperial College London, SW7 2AZ, UK (m.dougherty@imperial.ac.uk)

Abstract

Cassini magnetometer measurements have led to several important discoveries about the Saturnian system, including the southern plume at Enceladus, northern and southern magnetospheric near-planetary period oscillations and have confirmed the extreme axisymmetry of the internal field. The unique geometry of the end of mission proximal orbits provides an unprecedented opportunity to measure Saturn's intrinsic magnetic field at close distances to the planet, never before encountered. We hope to uncover the true nature of the internal magnetic field of Saturn, and in particular, to quantify the degree of asymmetry and to thus directly determine the true planetary rotation period. From magnetic field models based on measurements made during the proximal orbits, we hope to understand key aspects of Saturn's interior structure, such as the depth to the dynamo region.

EPSC Abstracts
Vol. 10, EPSC2015-782, 2015
European Planetary Science Congress 2015

Detection efficiency of microchannel plates to fluxes of high energy electrons similar to that in the Jupiter environment

M. Tulej (1), S. Meyer (1), M. Lüthi (1), D. Lasi (1), A. Galli (1) and P. Wurz (1)

L. Desorgher (2), K. Wojczuk (2), W. Hajdas (2), S. Karlsson (3) and L. Kalla (3)

(1) Space Research and Planetary Sciences, Physics Institute, University of Bern, CH-3012, Switzerland, (2) Paul Scherrer Institute, Lab Particle Physics, CH-5232 Villigen, Switzerland, (3) Swedish Institute of Space Physics, Space Campus 1, Kiruna, Sweden

(marek.tulej@space.unibe.ch / Phone: +41-31-631 44 05)

Abstract

High-energy high-rate electrons were measured by a multichannel plate (MCP) detector at the PiM1 beam line of the High Intensity Proton Accelerator Facilities located at the Paul Scherrer Institute, Villigen, Switzerland. The measurements provide the absolute detection efficiency of 8.5±0.8 % for e^- in the beam momenta range 17.5–345 MeV/c. The pulse height distribution determined from the measurements is close to an exponential function with negative exponent, indicating that the particles penetrated the MCP material before producing the signal somewhere inside the channel. Low charge extraction and modal gains of the MCP detector observed in this study are consistent with the proposed mechanism of the signal formation by penetrating radiation. A very similar MCP ion detector will be used in the NIM mass spectrometer of the PEP experiment currently developed for the JUICE mission of ESA to the Jupiter system, to perform measurements of the chemical composition of the exospheres of the Galilean moons.

1. Introduction

Particle Environment Package (PEP) is an instrument suite of the scientific payload of ESA's JUICE mission to the Jupiter system [1]. PEP will conduct remote global imaging of the Jupiter environment with in-situ measurements of particles including electrons, ions, energetic neutrals, and neutral gas in the particle energy range over nine decades (0.001 eV to 1 MeV). The results of the investigation will help understand the interaction of the Jupiter magnetosphere with Galilean moons. The neutral ion mass spectrometer (NIM) is a time-of-flight mass spectrometer, which is one of the particle instruments of PEP, and will be conducting chemical composition measurements of charged and neutral atoms, and molecules present in the exospheres of Jovian moons. The NIM instrument will record mass spectra within the mass range 1 – 1000 amu with a mass resolution ($m/\Delta m$) close to 1100 [2][3]. To achieve the required sensitivity, NIM uses a highly sensitive multichannel plate (MCP) ion detector. However, the presence of a substantial amount of high-energy particles (electrons, protons) trapped by Jupiter's magnetic fields (radiation belts) with the energy distribution exceeding hundreds of MeV both imposes high radiation tolerance requirements on the instruments and deteriorates their performance because of radiation-induced background signals. Understanding the interaction effects of this radiation with various materials is essential to optimally design NIM and its radiation shielding against penetrating radiation, and to interpret the obtained mass spectra. Although modelling techniques are continuously improving, not all the input parameters they require are easily accessible, in particular, the behaviour of detectors subjected to high-rate high-energy particle beams. Therefore, we performed the current radiation tests. They allowed us to identify the sensitivity of the MCP detector to radiation and the different signatures of particle species.

2. Experimental

The studies were conducted at the High Intensity Proton Accelerator Facility, PSI Villigen, Switzerland using the secondary beam line, PiM1 [4]. The PiM1 beamline is designed to deliver charged pions ($\pi^{\pm}$), electrons and positrons ($e^{\pm}$), muons ($\mu^{\pm}$) and protons (p) to the experimental area. Polarity and momentum of secondary particles are controlled by the currents in the magnet of the beam delivery system and can be changed by command. These particles are produced by the interaction between a

small fraction of the 590 MeV high intensity proton beam and a thin graphite target (M)[4].

The MCP detector used to measure electrons is placed in the vacuum chamber (Fig. 1) at a pressure of < 10^{-6}mbar. The e- beam with the beam momenta in the range 17.5–345 MeV/c was introduced to the detector by passing 2 mm thick aluminium window. Electron fluxes close to those expected in the Jupiter environment were applied. In parallel, the modelling by GRAS/Geant4 packages to test the prediction of beam rates and beam parameters at the MCP detector (Fig. 1).

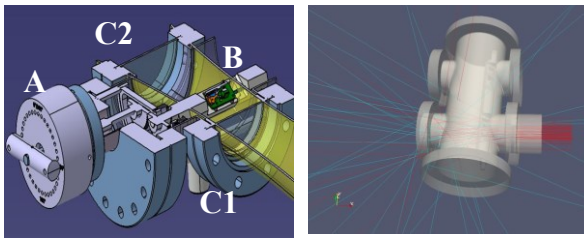

Fig.1. Left panel: Cut through the design drawing of the experimental vacuum chamber with a schematic envelope of the particle beam penetrating the vacuum chamber (yellow tubular feature): (A) rotating assembly, (B) the MCP detector, (C1) and (C2) entrance and rear aluminium window. Right panel: Visualisation from Geant4/GRAS simulation with primary e- beam of momentum 11.5 MeV/c.

To obtain the absolute detection efficiency of the MCP detector (η_{MCP}), the incident particle rate ($k_{Incident}$) at the front MCP and the MCP counting rates (k_{MCP}) were determined. The absolute MCP detection efficiency is defined as:

$$\eta_{MCP}(E_i) = 100 * \frac{k_{MCP}(E_i)}{k_{Incident}(E_i)}$$

The incident particle rate, $k_{Incident}$, [counts/sec] at the MCP surface was derived from the results of the diagnostic measurements by several beam detectors before the MCP experiment and by the ionisation chamber in real time. The measurements of the electrons by the MCP detector delivered the pulse height distribution (PHD) and means to determine the particle rates. The study yields the absolute detection efficiencies for e^- to be 8.5±0.8 % in the momenta range 17.5–345 MeV/c. The modelling results indicate that a decrease of the detector model gain can be expected for particle rates larger than 10^7counts/s, hence at least 10 times larger than those applied in the present investigation (Fig.2). There is no experimental evidence for a decrease of the MCP gain for the rates up to 10^6 counts /s. High-energy particles penetrate deeper into the MCP channel and extract less current from the detector, which still can be refilled without observable saturation of the detector. The modelling results predict also very well MCP gain dependence on electron rate under assumption that the MCP signal is produced by penetrating particles at some depth inside the MCP channel.

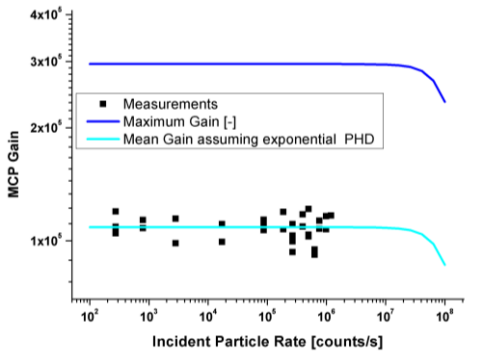

Fig. 2. Predictions of the MCP gain as function of the pulse rate determined from the paralysable-counter model are compared with the experimental results. The model predicts that for the MCP detector a possible saturation of the detector for the rates larger than10^7 particles/s is expected.

One of the important conclusions from this study is that at the investigated particle energies, even high rate of particles do not cause saturation of the detector. This can be of advantage when using this detector in Jovian environment. With the knowledge of the detection efficiency for penetrating electrons, both modelling and experimental investigation can be conducted to optimise radiation shielding against the radiation expected at the Jovian satellites.

Acknowledgements

The support of Swiss National Science Foundation and Swiss Space Office is kindly acknowledged.

References

[1] Grasset et al., (2013) *PSS*, 78, 1-21. [2] Abplanalp et al., (2009) *Adv. Space Res.*, **44**, 870-878. [3] Wurz et al., (2012) *PSS,* **74**, 264-269. [4] Hajdas et al., (2014) *JAMP* 2, 910-917.

EPSC Abstracts
Vol. 10, EPSC2015-819, 2015
European Planetary Science Congress 2015

Cassini SOI: Magnetometer data re-analysed

D. J. Southwood, J. N. Yates and M. K. Dougherty
(1) Physics Department, Imperial College, London, United Kingdom (d.southwood@imperial.ac.uk)

Abstract

The Cassini Saturn Orbit Insertion (SOI) on June 30 2004 marked Cassini's closest approach to Saturn in the mission so far. In advance of the proximal orbits it is appropriate to re-examine in preparation for the proximal orbit mission phase. SOI was the only occasion so far that Cassini has been on magnetic shells mapping to the A and B rings. At periapsis (r = 1.33 R_S, Λ = 15°) it was magnetically conjugate to the inner edge of the C ring. It cannot be ruled out that the observed field inside $L \approx 1.5$ is partly due to the longitude dependent internal field. g_{11} is a primary target and should show up in the data in special manner in part because of the spacecraft switch from retrograde to prograde motion around $L \sim 2$. Accordingly, for a source rotating at around 10.5-10.7 h., the spacecraft would sample azimuthal phase three times. This is illustrated here for the external cam source (G_{11}) where the effect is dramatic as the amplitude does change with r. We show in particular that the cam fields appear to extend into the regime over the rings.

EPSC Abstracts
Vol. 10, EPSC2015-835, 2015
European Planetary Science Congress 2015

Three dimensional aspects of magnetospheric circulation at Jupiter and Saturn

D. J. Southwood (1,2), E. Chané (2)
(1) Physics Department, Imperial College, London, UK, (2) Centre for mathematical Plasma Astrophysics, KULeuven, Belgium (d.southwood@imperial.ac.uk)

Abstract

Cowley et al. [2004] described flow in the giant planet magnetospheres by a Vasyliunas cycle transporting heavy material ionised in the inner magnetosphere outwards to eventual loss, mainly down-tail and a Dungey cycle whereby solar wind enters by day and the solar magnetic field connects to the magnetic flux in the polar cap through reonnection. We look at the latter Dungey cycle for the fast rotating magnetospheres of Jupiter and Saturn, emphasising particularly three-dimensional aspects.

1. Introduction

Cowley et al. [2004] described giant planet magnetospheric circulation with two cycles: the Vasyliunas cycle which carries heavy material from the inner magnetosphere outwards to eventual loss, mainly down-tail and a Dungey cycle where solar wind enters by day and reconnection connects the magnetic flux in the polar cap to the solar field. The recent discovery by the Cassini RPWS team [Gurnett et al. 2010] of a high latitude boundary they identify as the plasmapause is in our view the boundary between the Dungey and Vasyliunas regimes. The material originating in the Vasyliunas cycle starts near the magnetic equator and there is little reason for it to migrate off the equator as centrifugal effects keep it there. In the Dungey system is predominantly confined to the polar regions and the outermost closed flux tubes, solar wind material is likely to enter at high latitude far off the field line equator. Moreover, the lighter nature of the solar wind material that has entered means it can gain a much larger fraction of corotation speed. In this regime, the three dimensional structure of the circulation is important. The antisolar segment of the Dungey circulation is on open flux tubes and, in a fast rotator, the open tubes are swept towards the afternoon side of the magnetosphere and sunward flow on closed tubes is in the morning sector.

Dayside blockage and consequences

Using both theoretical estimations and a simulation parametrised for the jovian magnetosphere but with an aligned rotation and field symmetry axis like Saturn, we note that the morning side return path of the Dungey cycle is blocked in the equatorial plane by the combined effect of the slower moving heavy material of the Vasyliunas cycle and the subsolar magnetopause compression. As a result the lighter material in the outer regions coming from the Dungey tail reconnection region in the early morning region is both squeezed off the equator and moves outward. This results in

reconnection preferentially before noon and preferentially off the equator. The open tubes resulting from dayside reconnection can then move over/under the noon blockage and are accelerated down the afternoon side of the magnetosphere. Cassini data from high inclination orbits at high invariant latitude shows a reversal of magnetospheric-ionospheric stress near midday where there should also be distinct changes in auroral morphology.

Results

We present a scenario for the Dungey cycle with a strong dawn-dusk asymmetry and where most solar wind material entering near noon on an open tube is likely to leave the system by streaming down tail when that tube rotates into the evening/night sector. For Jupiter, we provide a natural explanation of the cushion region seen on the morning side. More controversially, we propose that for Saturn the entire Dungey system is pulsed at the 10.7h rate seen in magnetic field and radio emissions. Our scenario where much of the particle motion is off the equator goes some way to explain the maintenance of a slight difference in northern and southern rotation periods in the magnetic field pulsations and in the periodic planetary radio emission. Moreover it also explains the most intense radio emissions coming from the morning sector as well as the reported periodic injection of energetic particles from the early morning sector.

References

Cowley, S.W.H.. Bunce, E. J., and Prangé, R., Saturn's polar ionospheric flows and their relation to the main auroral oval, Annales Geophysicae 22: 1379–1394, 2004.

Gurnett, D.A., A. M. Persoon, A. J. Kopf, W. S. Kurth, M. W. Morooka, J.-E. Wahlund, K. K. Khurana, M. K. Dougherty, D. G. Mitchell, S. M. Krimigis, and N. Krupp (2010), A plasmapause-like density boundary at high latitudes in Saturn's magnetosphere, *Geophys. Res.Lett.*, 37, L16806, doi:10.1029/2010GL044466.

EPSC Abstracts
Vol. 10, EPSC2015-889, 2015
European Planetary Science Congress 2015

Probing Jupiter and Saturn: The prospects

T. Guillot
Laboratoire Lagrange, Observatoire de la Côte d'Azur, CNRS, Université de Nice-Sophia Antipolis, France

Abstract

In 2016 and 2017, the interiors of Jupiter and Saturn will be probed by the Juno and Cassini missions, respectively. Both will measure the planetary gravity and magnetic fields with unprecedented accuracy. In addition, Juno will probe Jupiter's deep atmosphere by radiometry in search of its elusive water. Altogether, the observational constraints used to construct interiors models will be improved extremely significantly. In parallel, the complexity of these models has been increasing steadily, due to the realization that their central core could erode over time, that double diffusive convection could set in and that the region in which helium separates from hydrogen is probably extended. Deriving much better constraints on the central core masses and global compositions of these planets will therefore require efforts to better examine the interplay between thermal cooling, mixing of elements, interior rotation, equations of state and dynamo generation. I will review the work in this direction. I will also show how seismology can ideally complement the constraints derived from the gravity field measurements.